archives
of thermodynamics
Vol. **42**(2021), No. 3, 255–278
DOI: 10.24425/ather.2021.138119

Design and computational fluid dynamics analysis of the last stage of innovative gas-steam turbine

STANISŁAW JERZY GŁUCH[a]*
PAWEŁ ZIÓŁKOWSKI[a]
ŁUKASZ WITANOWSKI[b]
JANUSZ BADUR[b]

[a] Gdańsk University of Technology, Faculty of Mechanical Engineering and Ship Building, Narutowicza 11/12, 80-233 Gdansk, Poland

[b] Institute of Fluid Flow Machinery Polish Academy of Sciences, Fiszera 14, 80-231 Gdansk, Poland

Abstract Research regarding blade design and analysis of flow has been attracting interest for over a century. Meanwhile new concepts and design approaches were created and improved. Advancements in information technologies allowed to introduce computational fluid dynamics and computational flow mechanics. Currently a combination of mentioned methods is used for the design of turbine blades. These methods enabled us to improve flow efficiency and strength of turbine blades. This paper relates to a new type turbine which is in the phase of theoretical analysis, because the working fluid is a mixture of steam and gas generated in a wet combustion chamber. The main aim of this paper is to design and analyze the flow characteristics of the last stage of gas-steam turbine. When creating the spatial model, the atlas of profiles of reaction turbine steps was used. Results of computational fluid dynamics simulations of twisting of the last stage are presented. Blades geometry and the computational mesh are also presented. Velocity vectors, for selected dividing sections that the velocity along the pitch diameter varies greatly. The blade has the shape of its cross-section similar to action type blades near the root and to reaction type blades near the tip. Velocity fields and pressure fields show the flow characteristics of the last stage of gas-steam turbine. The net efficiency of the cycle is equal to 52.61%.

*Corresponding Author. Email: stanislaw.gluch@pg.edu.pl

Keywords: Axial turbine; Blade design; Computational fluid dynamics; Last stage of low-pressure; Twisted blade

Nomenclature

c	–	absolute velocity, m/s
D	–	pitch diameter of the stage, m
h	–	specific enthalpy, kJ/kg
H_s	–	isentropic static enthalpy drop at the stage, kJ/kg
$l_s l_r$	–	length of the stator blade, length of the rotor blade, m
l_s	–	isentropic specific power, kJ/kg
l_u	–	specific work at the circumference, kJ/kg
$\dot{m}$	–	mass flow rate, kJ/s
N	–	power, MW
n	–	number of stage division into sections
p	–	pressure, MPa
r	–	radius, m
s	–	specific entropy, kJ/kgK
T	–	temperature, K
u	–	circumferential velocity, m/s
v	–	specific volume, m^3/kg
x	–	vapour quality
X	–	volumetric fraction or mole fraction
Y	–	mass fraction

Greek symbols

α	–	inlet angle between absolute velocity (c) and circumference velocity (u)
β	–	outlet angle between relative velocity (w) and circumference velocity (u)
Δ	–	difference
Σ	–	sum
η	–	efficiency
μ	–	mass flow capacity coefficient
ρ	–	reaction ratio
ω	–	rotation velocity, rpm

Subscripts and superscripts

bap	–	vacuum pressure
CCU	–	Carbon Dioxide capture unit
u	–	circumferential component
a	–	axial component
0	–	node before stator
1	–	node before rotor
2	–	node after rotor

Abbreviations

CFD	–	computational fluid dynamics
0D	–	zero-dimensional algebraic model of flow based on integral balances of mass, momentum and energy
3D	–	three-dimensional model based on differential equations, which requires complete geometry of a flow channel

1 Introduction

The work on turbine blade shaping dates back to the beginning of the last century [1], however, over the years new concepts have appeared [2,3]. Apart from the concepts themselves, a research tool was also developed which, starting from analytical tools [1], with time transformed into analyses including sophisticated numerical tools [4,5]. At present, turbine manufacturers are already based on a fully three-dimensional approach, both for solid-state stress analyses and for efficiency-enhancing flow analyses [6]. This paper refers to a turbine which is in the purely theoretical analysis phase, as the working fluid is the steam-gas produced in a wet combustion chamber. The concept of this circulation was developed in the works by Ziółkowski [7,8].

In [9] the numerical analysis of a four stage low pressure steam turbine was presented. The thermodynamic behavior of the wet steam was reproduced by adopting a real gas model. Geometrical features and flow-path details consistent with the actual turbine geometry were included in the analysis using simple models. Simple one-dimensional model of shrouded cavity was implemented, and its inclusion in the primary flow solver was described in detail. All these models were applied in the computation of the steam turbine, and computed spanwise distributions were compared to experimental ones at inlet/exit of the last stage. The models discussed in this paper were thought to be used as industrial tools suitable for turbomachinery design. They are aimed at capturing the relevant physics of some aspects which are usually neglected within the design process.

Paper [10] describes the features and analyses the results of a zero dimensional model for the design of high efficiency small size organic Rankine cycle (ORC) expanders. Starting from a previously developed 0D design tool (zero-dimensional algebraic model of flow based on integral balances of mass, momentum and energy) for radial ORC expanders [11] able to account for the specific loss correlations across the rotor, a 3D de-

sign procedure (three-dimensional model based on differential equations, which requires complete geometry of a flow channel) for very small expanders was developed with the purpose of achieving an improved design, mainly concerning the geometry of the flow channel and the number of blades. The 3D geometry of the rotor was imported in commercial computational fluid dynamics (CFD) packages. The improved design corresponds to the final fluid dynamics design of the rotor, with the improved blade geometry and a more suitable number of blades. The results of the 0D and 3D models applied to the reference case showed a satisfactory agreement, confirming the reliability of the 0D design tool as the basis for the definition of the overall geometry and working parameters of the machine.

Authors of [12] present the shape optimization of a three-dimensional nozzle and a two-dimensional (2D) turbine blade cascade based on CFD simulation of turbulent nucleating transonic wet steam flow in the corresponding flow passage. Both the liquid and gaseous phases were treated as continua and for each phase the conservation laws were solved together with proper source terms modeling the mass transfer and momentum exchange between two phases. A nonequilibrium condensation model based on classical nucleation and growth theory was utilized as well. Main conclusion of this work is that in analyzed cases k–ω SST (shear stress transport) turbulence model (two-equation eddy-viscosity) more accurately predicts the wet steam flow field in comparison to the well-known k-ε model for Moore's 'nozzle A' and Dykas's turbine blade cascade.

In [13] large-scale aerodynamic and structural interaction analysis was introduced to analyze steam turbine last stage blade. The two different kinds of unsteady flow analyses were carried out. The results show that the nozzle blade shock wave reflections on the rotor blade surface seem to be one of main origin that induce the flow unsteadiness and blade vibration in operating condition. The unsteady flow analysis of low load flow condition was carried out. This result shows the important flow features in the last stage. Robust data interpolation software was developed and proved to be able to be used in the present system. Existing measured data of the model steam turbine and the wheel box test facility was used to assume damping factors and to validate the unsteady flow analysis and computational solid dynamics result.

The recent technologies on developments and designs of last-stage long blades for steam turbines are explained in [14]. Technical features of last-stage long blades are high centrifugal force, high blade speed, 3D flow,

wet steam flow, and relatively large unsteady flow forces during low-load operations. Regarding future trends in last-stage long-blade technologies, recent studies cited in this chapter indicate that the accuracy of unsteady flow forces and blade vibration stresses in very low load conditions is being enhanced by employing state-of the-art CFD, computational solid dynamics (CSD), and fluid solid interaction (FSI) analysis. These new technologies, together with modern material science and fracture analysis based on strength of material science, will provide some breakthroughs to further increase the annulus areas. The redesign of existing blades for enhancement of low-load operation ranges employing these new technologies may bring more opportunities for steam turbine power plants because these power plants need to be operated to control electrical grid fluctuations due to the increase in the numbers of renewable-energy power plants.

Authors of [15] proposed procedure for selection of optimum degree of partial admission depending on the tip clearance. A case study has been presented for a microturbine designed for operation in a micro combined heat and power (micro-CHP) unit running with HFE 7100 working fluid (hydrofluoroethers). A series of CFD simulations were performed to examine the turbine performance more precisely and to determine some of the component loss correlations. Authors of [16] used CFD to optimize an axial turbine for a small scale ORC waste heat recovery system. In [17] CFD was used to compare impulse and reaction stages in ORC power plant.

Authors of [18] performed numerical study aimed at investigating the steady and unsteady interactions between the components of a two-stage axial turbine. They found out that the expansion rate and flow range are mainly controlled by the first stage. First stage wakes, secondary flows and vortices cause flow perturbations and losses to the second which persist downstream. Since the flow field is very affected by the wakes and vortices, a better design has to account for the optimum clocking position. In order to reduce the pressure loss due to the first stage tip leakage and vortices, a better flow control should be managed in the first rotor and second nozzle guide vanes (NGV) and consider the effects of the gap between blade-rows.

Numerical studies have been conducted in [19] to understand the rotating instability previously experimentally identified at low mass flow rates in a model steam turbine stage. An initial CFD analysis using a time-domain Reynolds-averaged Navier–Stokes (RANS) equations solver is able to capture a large scale separated flow pattern, which is comparing well with the experimentally observed one. The 3D vertical flow pattern observed in the

experiment is reproduced in the 3D calculation. The results consistently show that a rotating pattern non synchronized with the rotor speed exists at low mass flow conditions. The dominant frequency for the tip section identified by the Fourier transform is higher (by 50%) than the experimental value and shifts when the mass flow rate is changed. The results suggest that the rotating speed of the patterns as seen in the stationary frame of reference is about a half of the rotor rotation speed. On the other hand, the near hub section is much more stable with no clearly identifiable rotating patterns found at low mass flow conditions.

Neural networks could aid CFD in the stage design. Authors of [20] presented the application of neural networks as an alternative approach for expensive calculations. Neural networks could be used in stage modeling when network is taught at similar geometry [21]. In some cases deep learning could be used with success when data is incomplete [22].

The aim of the work is to adopt the free vortex law to the gas-steam turbine, and further to analyze the nature of the flow using CFD tools. Use of gas-steam as working fluid is a new concept. Analysis of the results would allow to preliminary determine possible challenges in construction of this kind of turbine and recognize differences between analyzed stage and conventional steam turbine stage. Subject of research is the geometry and operation of the last stage of low pressure part of innovative gas steam turbine. Construction of the last stage and control stage [23] are the most demanding challenges for turbomachinery engineers. In this type of turbine the working fluid consists of about 90% water steam and 10% carbon dioxide (CO_2). Effect of working fluid on cycle performance is presented in [24]. Conditions at the last stage are similar to these which occur in conventional steam turbines, but pressure and temperature are slightly higher, thus condensation does not occur. Geometry of rotor blade of conventional last stage of steam turbine is presented in Fig. 1. Outlet area has to be big enough to allow for reasonable outlet velocity from turbine. Higher outlet velocity contributes to the increase of outlet losses. Due to the difference in peripheral velocity the blade has to be twisted. Reaction ratio differs form 0.1 at the hub to even 0.9 at the shroud. Because of that inlet (α) and outlet (β) angles have different values at the hub and the shroud. Different laws of twisting, such as free vortex, could be applied in the design. Blades at the bottom and at the top have to be constructed from different profiles. Operation of stage initially designed by 0D approach should be checked by CFD analysis.

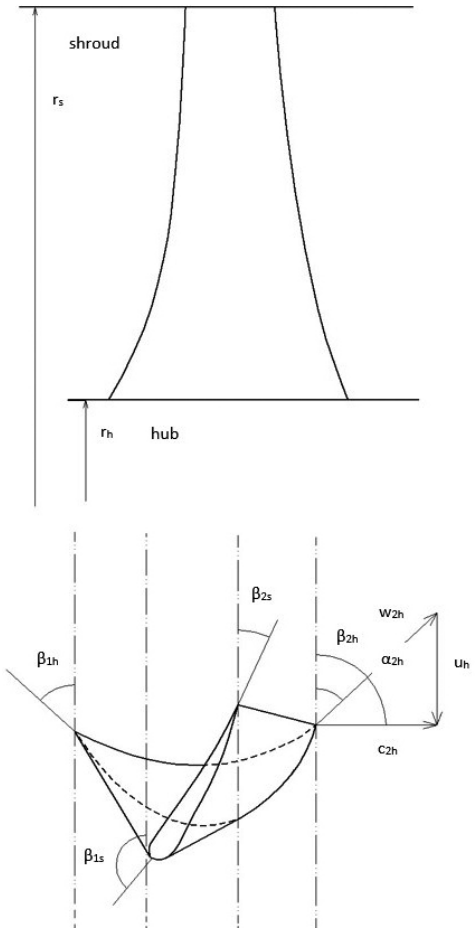

Figure 1: Schematic diagram of the last stage blade and the angles α and β for different height level, where r_s – radius at tip of blade net the shroud, r_h – radius with hub connection, β_{1h} – relative velocity degree after stator at the hub, β_{1s} – relative velocity degree after stator at the shroud, β_{2h} – relative velocity degree after rotor at the hub, β_{2s} – relative velocity degree after rotor at the shroud, α_{2h} – absolute velocity degree after rotor at the hub, c_{2h} – absolute velocity at the hub, w_{2h} – relative velocity at the hub, u – circumferential velocity.

2 The case under consideration

This gas-steam turbine consists of high-pressure and low-pressure part. Figure 2 shows a diagram of a compact gas-steam power plant, where the key element is the original wet combustion chamber (WCC), which is a steam-

gas generator. In this chamber (WCC), the product of the oxygen combustion of gases, combined with the 'nano production' of steam, is a working fluid containing about 80–90% steam and 20–10% CO_2. The exact data are shown in Table 1. It is therefore important to separate water vapor from CO_2 accordingly. The original idea was proposed in [7]. First, the compression of oxygen produced in the air separation unit (ASU) is shown (CO_2 nodes 1–2). It goes to a wet combustion chamber, where stoichiometric combustion of methane occurs. The mixture produced in this way is cooled with water, which is transformed into steam. Another important process of this solution is the expansion of the working fluid in a high-temperature gas turbine (GT) (nodes 3–4 in Fig. 2), followed by the expansion of the flue gas in conditions below atmospheric pressure (GT^{bap}) (nodes 4–1^{bap}). The regeneration heat exchanger (HE) then heats water (nodes 9–10) and cools the exhaust gas (1^{bap}–2^{bap}). The mass flow rate of flue gases, after the transfer of thermal energy, goes to the spray-ejector condenser, where it is compressed to the state specified at node 5. However, the water driving the nozzle and the flue gases taken from the node 2bap are on a single line, with a cross-section of 3^{bap}–15. The cooling and compressing water and the condensed flue gases are mixed between nodes 3^{bap}–4^{bap} (or 15–16).

Table 1: Parameters of mixture and computational domain used in CFD simulation of a last turbine stage.

Inlet temperature, $T_0 = 610$			K
Rotation velocity, $\omega = 3000$			rpm
Outlet total pressure, $p_2 = 0.007955$			MPa
Inlet total pressure,$p_0 = 0.016225$			MPa
X_{CO_2}	X_{H_2O}	X_{N_2}	$\sum X$
0.0894	0.9084	0.0022	1
Y_{CO_2}	Y_{H_2O}	Y_{N_2}	$\sum Y$
0.1933	0.8037	0.003	1

It can be assumed that the complete mixing of the fluid has already taken place at node 4^{bap}, the thermodynamic parameters of which become the same as in the node 16. Thus, in the spray-ejector condenser (SEC), first the water and flue gases expand, then they are mixed with each other. Finally, in the diffuser, the pressure is raised to about 0.1MPa (node 5). The purpose of the applied modification is to reduce the dimensions of the condenser compared to a solution without water injection on the working fluid flowing out of the turbine.

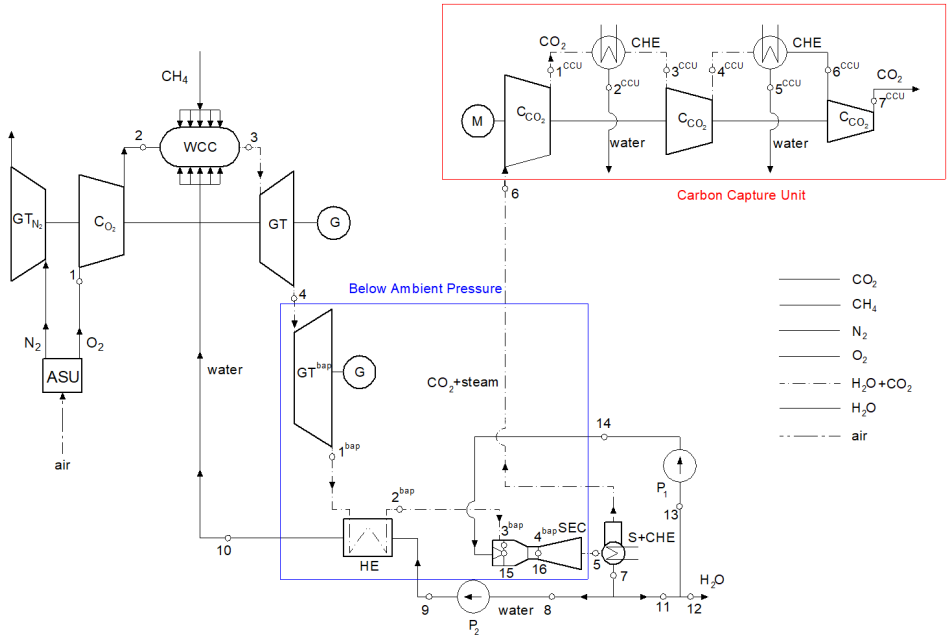

Figure 2: The double Brayton cycle with oxy-combustion and CO_2 capture (DBCOCC), where WCC – wet combustion chamber, ASU – air separation unit, C – compressor, CCU – carbon capture unit, CHE – cooling heat exchanger, C_{CO2}–CO_2 compressor, G – generator, GT+GT^{bap}– gas turbine divided into two parts, GT_{N2} – expander N2, HE – heat exchanger, M – motor, P_1 – supply water pump, P_2 –water pump for cooling combustion chamber, SEC – spray ejector condenser, S+CHE – separator and condensate-cooler heat exchanger.

Another device is the heat exchanger joined with a separator, in which the resulting mixture is cooled, and carbon dioxide and part of steam are separated from water (S+CHE – separator and condensate-cooler heat exchanger). Clean and cooled water flows out at node 7 and is then directed to two pumps — namely, low-pressure P_1 and high-pressure P_2. Some of the water produced during combustion condensates into the spray-ejector condenser; thus, a certain excess of the working fluid has been created, which is removed from the cycle at node 12. The P2 pump, on the other hand, ensures that the pressure is raised to 0.4 MPa and that water is directed to cooling the combustion chamber.

The last process occurring in the double Brayton cycle with oxy- combustion and CO_2 capture is carbon capture, which takes place in a series of devices (carbon capture unit – CCU). Starting from point 6, the mixture

of CO_2 and steam is compressed and the water is gradually condensed in subsequent exchangers (CHE – cooling heat exchanger). As can be seen in the next set of devices – CO_2 compressors and cooling heat exchangers – (CCO2+CHE), the CO_2 pressure increases and the water content decreases. The final result is pure carbon dioxide at 8 MPa at node 7^{CCU}.

It is also worth noting that a mixture of steam and carbon dioxide is generated in a wet combustion chamber, which then expands in the turbine. For such a medium, the adaptation of a gas turbine due to temperatures and the adaptation of a steam turbine due to its size in the low-pressure part may be considered. However, in this situation, it is most justified to design a brand-new expander that will combine the advantages of both devices. An important element of the system is the air separation unit (ASU), which is described in the next section.

Figure 3 presents the shape of the last expander stage to ensure optimal use of the working fluid enthalpy in GT+GT^{bap}. The turbine consists of one high pressure housing and one low-pressure, two outlet housing. This new type of turbine combines advantages of gas turbines and steam turbines [25, 26]. Power plant which operates in this cycle is an alternative to high-temperature reactor (HTR) as reliable and zero-emission power source [27].

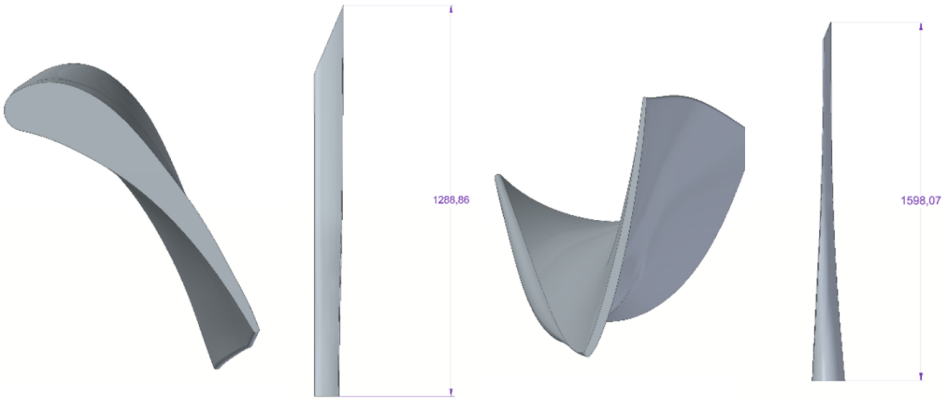

Figure 3: Stator and rotor blade – view from the top and front, respectively.

The number of stages of the high and low-pressure parts of the turbine (27 and 6 stages in both directions, respectively) were determined, together with the kinematics and velocity vectors for subsequent stages of the axial turbine. The low-pressure part has two outlets. The length of the rotor blade of the last stage is 1.587 m (Fig. 3). The design process takes into

account the law of variation of the velocity peripheral component of the working medium along the radius of the turbine blade and it is conducted in a discrete way so that a 3D drawing of the resulting geometry can be performed. The circumferential velocity varies from 262 m/s near the blade hub to 771 m/s near the blade tip.

Figure 3 shows a geometry of the stator and rotor blade designed based on the free vortex law. The last stage of turbine is always a peculiar one, not only it is challenging from the material strength point of view, but also regarding the fluid flow. Numerical analysis of this particular case also provides difficulties. To ensure that simulation will be performed correctly the discretization of the analyzed domain must be done properly with inclusion of crucial elements. For this purpose, hexahedral mesh was chosen, as one that provides excellent accuracy and relatively low elements count. In this case to perform calculations in reasonable time period a mesh consisting of 4 000 000 hexahedral elements was used. Mesh limits were set on the maximum face angle – 165°, minimum face angle – 15°, connectivity number – 12, maximum and minimum volume ratio – 10 and 0, and maximum edge length ratio – 500.

Cross section through the domain was shown in Fig. 4, on the left part the stator's blade mesh is portrayed and on the right side is the mesh used on rotor blades. Mesh used in rotor stage was finer due to more complex phenomena's occurring compared to stator hence for better reproduction of real processes it is necessary. In this paper only one channel was modelled and in circumferential direction periodic boundary condition was implemented to imitate the impact of other turbine blades on the fluid flow without unnecessarily increasing elements count.

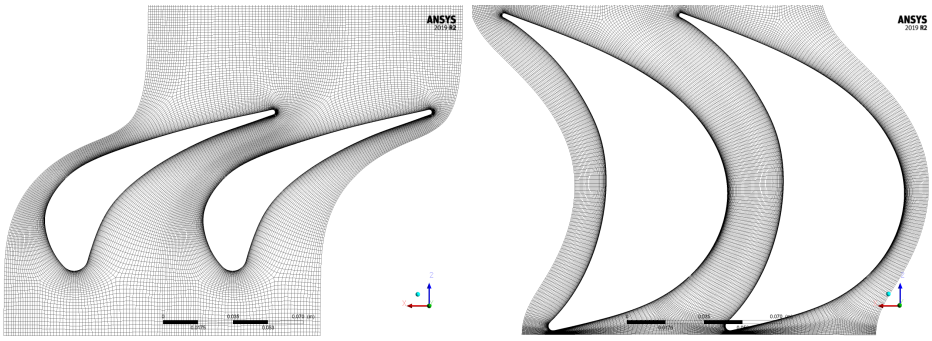

Figure 4: Mesh used in numerical simulation, respectively stator and rotor on the left and right side of the figure.

3 Mathematical model

The calculation is performed in two steps, namely: 1) determination of the shape of the last stage based on the free vortex law; 2) calculation of the flow based on CFD tools.

3.1 Twisted blade model

Kinematics of the stage undergoes significant changes as we disregard the assumption that the channel high following the radius is homogeneous. In fact, the flow fields change with the radius. In order to increase the efficiency of the turbine, shape of the blades must be adjusted to the changing flow. It is accomplished by changing the inlet (α) and outlet (β) angles angles in order to adjust the blade shape to the changing circumferential speed u. The twisting was performed using the free vortex method due to Perycz presented in [28], as this method has been described most precisely. However, in the further part of this work we will also refer to Szewalski's proposal [1–3].

Usually, the law of coiling of the second blade, i.e. the law of variation of the circumferential component of the speed of the working fluid in radial direction, is rather suitable in a discrete form, and differently for the inlet to the vane channel and for the outlet. In engineering practice, it is assumed that the circumferential velocity compoent at the outlet is to be as low as possible and should not be increased unnecessarily due to the decrease in efficiency by dissipation of kinetic energy of the medium operating at the outlet [28]. Thus, the free vortex procedure is based on the free vortex method. The stage was divided into 15 sections. Reaction ratio (ρ) at the root was assumed as 0.1 to avoid ventilation work during partial loads. The calculation is carried out in an iterative manner and the parameter to be compared is the mass flow, as the value of the sum of contributions ($\Delta\dot{m}$) from the individual sections of the discernment shall be equal to $\dot{m} = 91.15$ kg/s.

The initial assumptions for a twisted stage are collected in Table 2. In turn, the assumed parameters of the step needed to carry out the calculation of the twisting for selected sections of the discretisation are presented in Table 3. In Table 4 presents the results of calculations for the five divisional sections. Section number 8 is located on the pitch diameter. Due to very large changes in the value of circumferential velocity (u) there are large changes in reactivity, angles and velocity along the radius. The value of

circumferential speed varies from 262 m/s to 771 m/s. The sound velocity in this area fluctuates around 440 m/s.

Table 2: Initial assumptions regarding twisted stage.

Parameter	Unit	Value
Initial reaction ratio, ρ_n	–	0.1
Radius at the hub of the stator, r_{n1}	m	0.820115209
Radiuos at the hub fo the stator, r_{n2}	m	0.820115209
Total enthalpy drop, H_{sc}	kJ/kg	178.6120643
Static enthalpy drop, H_s	kJ/kg	165
Lenghth of stator blade, l_s	m	1.293335645
Lenghth of rotor blade, l_r	m	1.578019487
Mean diameter, dm	m	3.21825
Rotation velocity, ω	rad/s	314.1592654
Angle at the mean diameter of the stator, α_1	°	22.5
Inlet pressure, p_0	MPa	0.016255325
Inlet enthalpy, h_0	kJ/kg	2695.346123
Inlet enthropy, s_0	kJ/(kgK)	8.254181075
Mass flux, $\dot{m}$	kg/s	91.15
Inlet velocity, c_0	m/s	164.9973594
Number of calculation sections, n	–	15
Length of calculated stator section, Δl_k	m	0.086222376
Lenght of calculated rotor section, Δl_w	m	0.105201299
Angle at the hub of the stator, α_1	°	11.92069374

Table 3: Assumptions regarding chosen sections of a twisted blade.

Parameter	1	4	8	12	15
Velocity coefficient at the stator, μ_1	0.940	0.940	0.940	0.940	0.940
Velocity coefficient at the rotor, μ_2	0.940	0.940	0.940	0.940	0.940
Flow capacity coefficient at the stator, φ	0.935	0.950	0.950	0.950	0.950
Flow capacity coefficient at the rotor, ψ	0.925	0.935	0.935	0.935	0.935

It should be noted that near the hub the blade is impulse at the foot and features extremely high reaction ratio at the apex. The minimum reaction ratio (ρ) of 0.1 is at the hub. This value should not fall below 0.1 so that there is no negative degree of reaction value at the loss of partial power. Reaction ratio near the shroud is as high as 0.89. Figures 5–7 show the velocity triangles for selected divisional sections.

Table 4: Results obtained in the twisted stage.

Parameter	Unit	1	4	8	12	15
Radius at the bottom of calculated stator section, r_1	m	0.8632	1.1218	1.4667	1.8116	2.0703
Radius at the bottom of calculated rotor section, r_2	m	0.8727	1.1883	1.6091	2.03	2.3455
Reaction ratio, ρ	–	0.1906	0.5221	0.7152	0.8084	0.8503
Circumferential velocity, u	m/s	274.17	373.32	505.52	637.72	736.87
Inlet angle at the stator, α_1	°	14.661	19.008	24.95	30.089	33.623
Axial velocity, c_{1s}	m/s	529.8	413.9	328.02	277.18	251.01
Absolute velocity after stator, c_1	m/s	495.38	393.2	311.6	263.32	238.46
Outlet area, $DeltaA_1$	m^2	0.4677	0.6078	0.7946	0.9814	1.1216
Mass flux, $\Delta\dot{m}$	kg/s	2.471	3.896	5.807	7.57	8.85
Outlet angle at the rotor, β_2	°	20.988	19.127	16.476	13.861	12.262
Circumferential specific work, l_u	kJ/kg	146.15	150.15	144.25	135.38	126.99
Isentropic specific work, l_s	kJ/kg	158.04	156.09	154.27	153.28	152.75
Efficiency of the section, η	–	0.9247	0.9619	0.935	0.8832	0.8313
Power of the section, ΔN_s	MW	0.3905	0.608	0.8959	1.1604	1.3513

The main result, apart from the thermodynamic parameters, is the number of axial stages, respectively: 27 stages for the high-pressure part (GT) and 6 stages for the low-pressure part (GT^{bap}) as shown in Fig. 3. The length of the rotor blade of the last stage reached $l_s = 1.57$ m and this is a value comparable to the blades that operate in the newest steam unit in Kozienice Power Plant (placed in eastern Poland). In addition, it should be mentioned that this turbine is double-housed: high pressure and low-pressure parts, and that the low-pressure part has double outlet.

3.2 CFD model in 3D simulation

Steady-state Reynolds averaged Navier–Stokes (RANS) calculations were performed with the help of the commercial CFD code for turbomachinery applications, Ansys CFX [29] using second order spatial discretization with an automatic time step. The Menter [30] k-ω SST (shear stress transport) turbulence model was used. The imposed set of boundary conditions consists of total pressure and total temperature at the inlet, average static pressure at the outlet and rotational speed of the rotor domain. The frozen rotor technique is assumed to tackle the interface between the station-

ary and rotating domains. The rotor blades are unshrouded. The working fluid was described using through the NIST Refprop database (*Reference Fluid Thermodynamic and Transport Properties*) [31]. This model is resolving a set of basic equations, namely mass, momentum and energy balance equations for the fluid and energy dissipation equations.

3.3 Analysis of results

It is worth noting the large velocity changes along the pitch diameter. At the hub the velocity vectors that represent a low degree of reaction are clearly visible, Fig. 5. At the apex the most different velocity triangle, Fig. 7, can be observed.

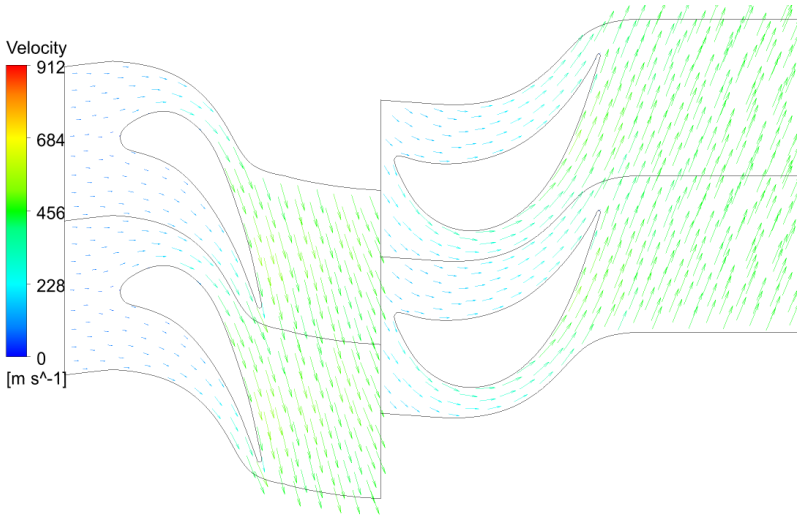

Figure 5: Velocity vectors at the hub.

In Fig. 5 we can see velocity vectors at the hub. This part of stage has a low reaction ratio (0.1) and operates like an action stage. Most of expansion takes place at the rotor. Edge trail can be observed. Vortexes are not present. Velocity vectors at the mid span are presented in Fig. 6.

This part of turbine has a high reaction ratio (0.7), which is higher than in conventional impulse stage. Most expansion takes place at the rotor, what could be observed by values of velocity vectors. Vortexes does not appear. Flow conditions at the shroud are presented in Fig. 7. Reaction parameter is extremely high here (0.85). Radial change of shape of channel

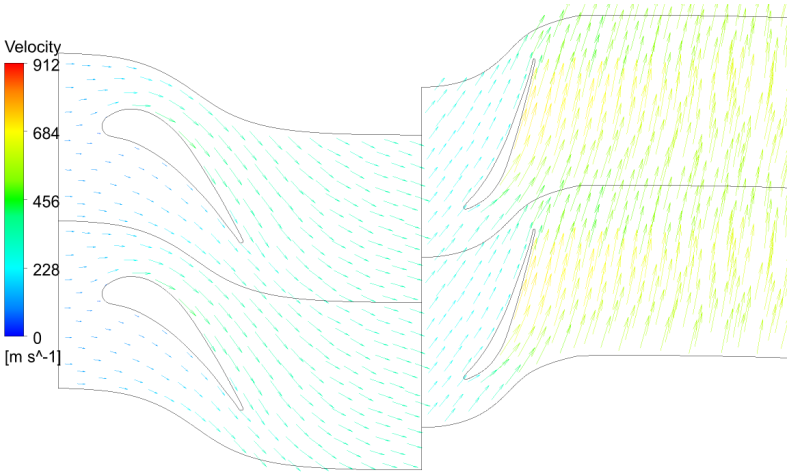

Figure 6: Velocity vectors at the mid-span.

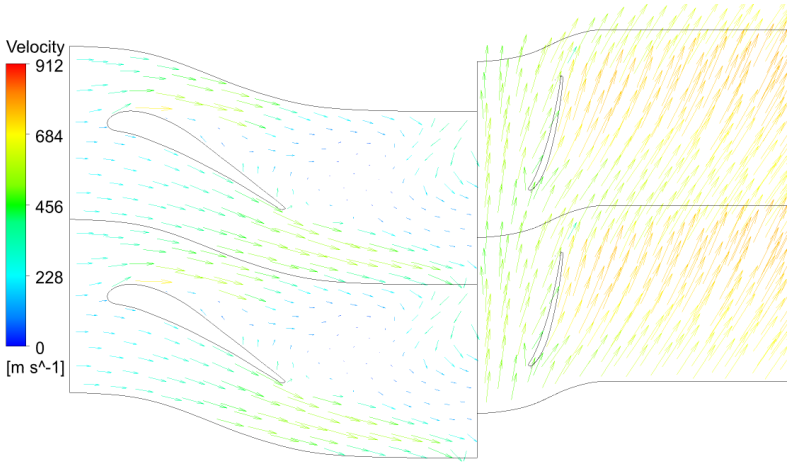

Figure 7: Velocity vectors at the shroud.

could be origin of vortex which could be observed. This part of stage should be redesigned with the use of optimization algorithms.

In Fig. 8 we can see contours of Mach number at the hub and at the mid span. In Fig. 9 Mach number contours at the top of the blade are presented. Velocity at the hub is close to 1 Ma, but this value is not surpassed. There is no need to apply supersonic profiles at the hub. At the mid span velocity reach safe value of 0.76 Ma, however velocity at the shroud exceeds 1 Ma. This area has to be adapted for supersonic flows.

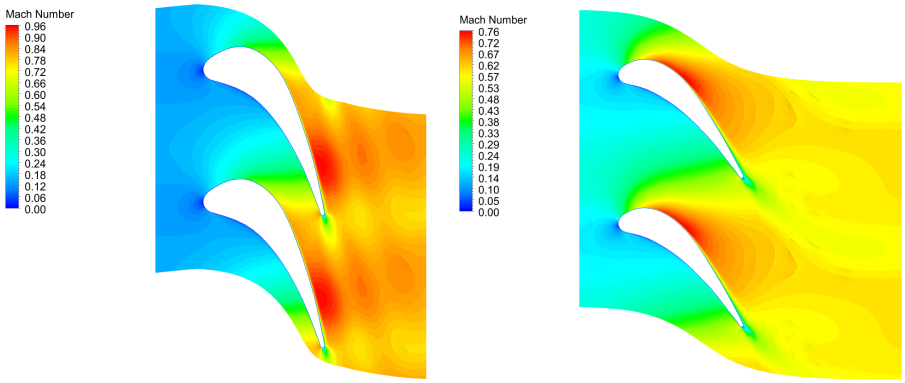

(a) (b)

Figure 8: Mach number contours: a) at the hub and b) the mid-span.

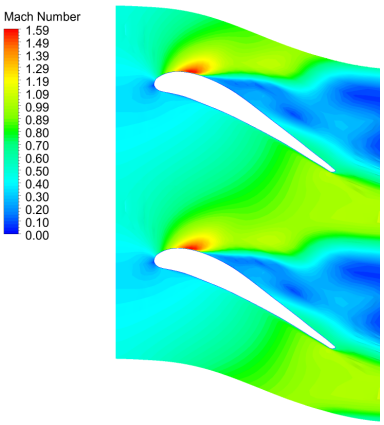

Figure 9: Mach number at the shroud.

Pressure contours at the hub and at the mid span are presented in Fig. 10. In Fig. 11 pressure contours at the top of the blade can be seen. In all three cases pressure on the suction side of profile is lower than on the pressure side. Areas of higher pressure does not appear even at the shroud. Vortex, which could be observed in velocity vectors image could not be observed in pressure contour image.

In Fig. 12 we can see temperature contours at the hub and at the mid span. In Fig. 13 temperature contours at the top of the blade are presented. Effect of edge trails could be observed in all three images. Area of increased temperature inside vortex at the shroud could be observed.

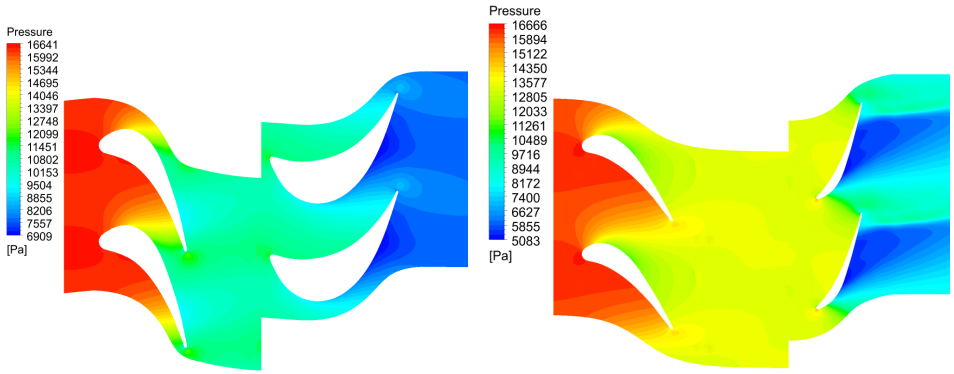

(a) (b)

Figure 10: Pressure contours at the hub a) and at the mid-span b).

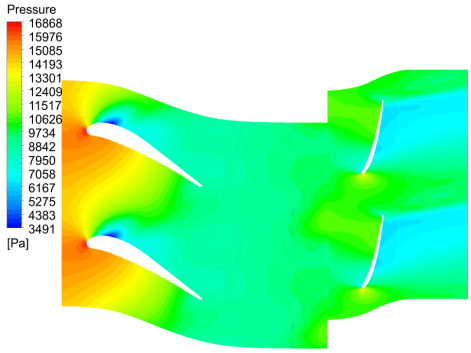

Figure 11: Pressure contours at the shroud.

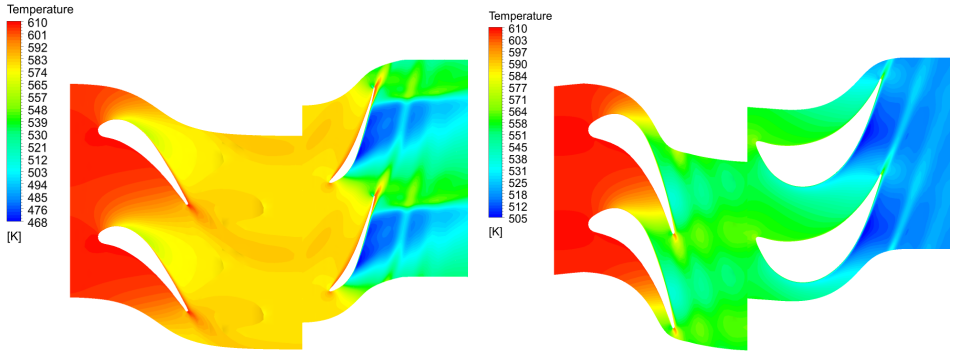

(a) (b)

Figure 12: Temperature contours at the hub a) and at the mid-span b).

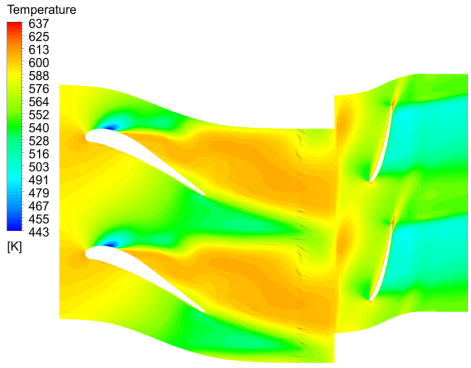

Figure 13: Temperature contours at the shroud.

Static entropy contours shown in Figs. 14 and 15 indicate a high intensity of flow losses in shroud section of stator and rotor rows. In the mid-span and hub section the profile losses can be observed.

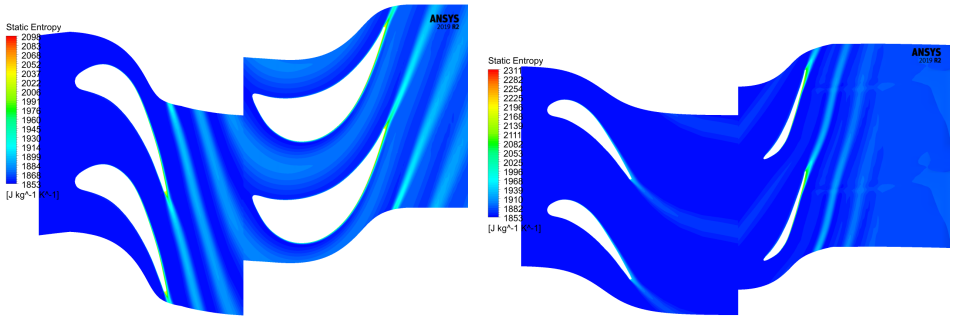

(a) (b)

Figure 14: Static entropy contours at the hub a) and at the mid-span b).

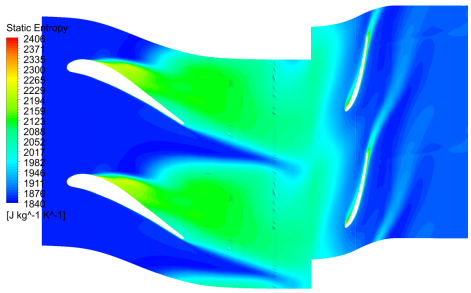

Figure 15: Static entropy contours at the shroud.

Fig. 16 shows the distribution of loading through the rotor passage. The blade is more loaded closer to trailing edge of the blade. The pressure profiles in the hub is regular during the entire axial distance. In the mid-span section occurs the higher pressure difference between suction and pressured side of the profile.

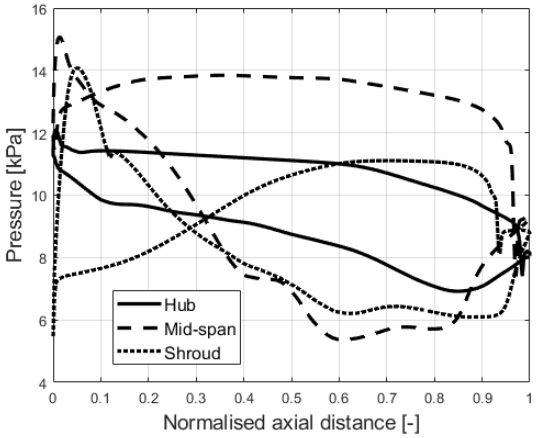

Figure 16: Rotor blade loading at the hub, mid-span and shroud.

In Fig. 17 streamlines inside stage could be observed. In Fig. 18 static entropy contours and temperature contours can be seen. It can be noted,

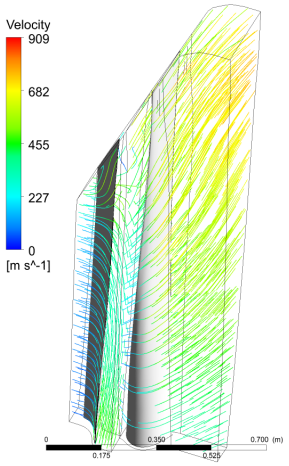

Figure 17: Streamlines in the stage.

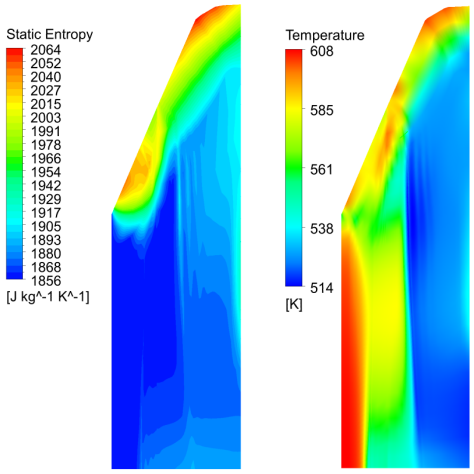

(a) (b)

Figure 18: Static entropy contours in the stage a) and temperature b).

that most of the losses take place at the very top of the stage. Most of the stage work as intended, so the optimisation should focus on geometry near the shroud.

4 Conclusions

The results obtained by the analytical method – free vortex – and the numerical method using computational fluid dynamics codes were compared. This is the first work which analyses flow of steam and carbon dioxide mixture. The analytical method allowed to determine the geometry of spatially twisted and trimmed vanes of the guide and rotor blades. Additionally, thermodynamic parameters, which were boundary conditions for computational fluid dynamics simulations, were determined using analytical methods. This information (geometry and thermodynamic parameters) was used as input data for CFD analysis. The velocity vectors and temperature fields showed a satisfactory agreement between the numerical and analytical calculations in the hub and mid-span (split radius) areas only. However, more attention should be focused on the essential differences that apply to the mass flow and the phenomena occurring at the top of the blade. The mass flow in analytical and in numerical terms reached 25% differences. In addition, CFD simulations showed ventilating operation in the upper edge area of

both rotor and stator blades, resulting in temperature rise and significant entropy generation in this area. On the basis of the analysis, it should be concluded that the current shape of the channel should be redesigned in order to achieve the assumed mass flows of the working medium while maintaining the assumed efficiency. Presented analysis is basis for further optimization with use of optimization algorithms. Result show that it is feasible to construct the last stage with 1.57 m long rotor blade for new gas-steam zero emission power plant.

Acknowledgements The research leading to these results has received funding from the Norway Grants 2014–2021 via the National Centre for Research and Development. Article has been prepared within the frame of the project: "Negative CO_2 emission gas power plant" – NOR/POLNORCCS/NEGATIVE-CO2-PP/0009/2019-00 which is co-financed by programme "Applied research" under the Norwegian Financial Mechanisms 2014–2021 POLNOR 2019 – Development of CO_2 capture solutions integrated in power and industry processes.

Received 28 February 2021

References

[1] Szewalski R.: *Rational Blade Height Calculation in Action Turbines*. Czasopismo Techniczne (1930), 1, 83–86 (in Polish).

[2] Szewalski R.: *A novel design of turbine blading of extreme length*. Trans. Inst. Fluid-Flow Mach. **70–72**(1976) 137–143.

[3] Szewalski R.: *Present Problems of Power Engineering Development. Increase of Unit Power and Efficiency of Turbines and Power Palnts*. Ossolineum, Wrocław Warszawa Kraków Gdańsk 1978 (in Polsih).

[4] Gardzilewicz A., Świrydczuk J., Badur J., Karcz M., Werner R., Szyrejko C.: *Methodology of CFD computations applied for analyzing flows through steam turbine exhaust hoods*. Trans. Inst. Fluid-Flow Mach. **113**(2003), 157–168.

[5] Knitter D., Badur J.: *Coupled 0D and 3D analyzis of axial force actiong on regulation stage during unsteady work*. Systems **13**(2008), 1/2 Spec. Issu., 244–262 (in Polsih).

[6] Knitter D.: *Adaptation of inlet and outlet of turbine for new working conditions*. PhD dissertation, Inst. Fluid Flow Mach. Pol. Ac. Sci., Gdańsk, 2008 (in Polish).

[7] Ziółkowski P.: *Thermodynamic analysis of low emission gas-steam cycles with oxy combustion*. PhD dissertation, Inst. of Fluid Flow Mach. Pol. Ac. Sci., Gdańsk 2018 (in Polish).

[8] Ziółkowski P., Badur J.: *A study of a compact high-efficiency zero-emission power plant with oxy-fuel combustion*. In: Proc. 32nd Int.Conf. on Efficiency, Cost, Optimization, Simulation and Environmental Impact of Energy Systems, ECOS, Wroclaw, 2019 (W. Stanek, P. Gładysz, S. Werle, W. Adamczyk, Eds.), 1557–1568.

[9] Rubechini F., Marconcini M., Arnone A., Stefano C., Daccà F.: *Some aspects of CFD modelling in the análisis of a low-pressure steam turbine*. In: Power for Land, Sea, and Air, Proc. ASME Turbo Expo, Montrèal, May, 14–17 2007, GT2007-27235.

[10] Fiaschi D., Manfrida G., Maraschiello F.: *Design and performance prediction of radial ORC turboexpanders*. Appl. Energ. **138**(2015), 517–532.

[11] Fiaschi D., Innocenti G., Manfrida G., Maraschiello F.: *Design of micro radial turboexpanders for ORC power cycles: From 0D to 3D*. Appl. Therm. Eng. **99**(2016), 402–410.

[12] Noori Rahim Abadi M.A., Ahmadpour A., Abadi S.M.N.R., Meyer J.P.: *CFD-based shape optimization of steam turbine blade cascade in transonic two phase flows*. Appl. Therm. Eng. **112**(2017), 1575–1589.

[13] Tanuma T., Okuda H., Hashimoto G., Yamamoto S., Shibukawa N., Okuno K., Saeki H., Tsukuda T.: *Aerodynamic and structural numerical investigation of unsteady flow effects on last stage blades*. In: Microturbines, Turbochargers and Small Turbomachines, Steam Turbine, Proc. ASME Turbo Expo, Montrèal, June 15–19, 2015, GT2015-43848.

[14] Tanuma T.: *Development of last-stage long blades for steam turbines*. In: Advances in Steam Turbines for Modern Power Plants (T. Tanuma, Ed.). Woodhead, 2017, 279–305.

[15] Klonowicz P., Witanowski Ł., Suchocki T., Jedrzejewski Ł., Lampart P.: *Selection of optimum degree of partial admission in a laboratory organic vapour microturbine*. Energ. Convers. Manage. **202**(2019), 112189.

[16] Witanowski Ł., Klonowicz P., Lampart P., Suchocki T., Jedrzejewski Ł., Zaniewski D., Klimaszewski P.: *Optimization of an axial turbine for a small scale ORC waste heat recovery system*. Energy **205**(2020), 118059.

[17] Zaniewski D., Klimaszewski P., Witanowski Ł., Jedrzejewski Ł., Klonowicz P., Lampart P.: *Comparison of an impulse and a reaction turbine stage for an ORC power plant*. Arch. Thermodyn. **40**(2019), 3, 137–157

[18] Touil K., Ghenaiet A.: *Characterization of vane-blade interactions in two-stage axial turbine*. Energy **172**(2019), 1291–1311.

[19] Zhang L.Y., He L., Stuer H.: *A numerical investigation of rotating instability in steam turbine last stage*. In: Power for Land, Sea, and Air, Proc. ASME Turbo Expo, Vancouver, June 6–10, 2011, GT2011-46073, 1657–1666.

[20] Butterweck A., Głuch J.: *Neural network simulator's application to reference performance determination of turbine blading in the heat-flow diagnostics*. In: Intelligent Systems in Technica and Medical Diagnostics (J. Korbicz, M. Kowal, Eds.), Advances in Intelligent Systems and Computing, Vol. 230. Springer, Berlin Heidelberg 2014, 137–147.

[21] Głuch J. Drosińska-Komor M.: *Neural Modelling of Steam Turbine Control Stage*. In: Advances in Diagnostics of Processes and Systems (J. Korbicz, K. Patan, M. Luzar, Eds.), Studies in Systems, Decision and Control, Vol. 313. Springer, 2021, 117–128.

[22] Głuch J., Krzyżanowski J.: *Application of preprocessed classifier type neural network for searching of faulty components of power cycles in case of incomplete measurement data*. In: Power for Land, Sea, and Air, Proceed. ASME Turbo Expo, Amsterdam, June 3–6, 2002, GT2002-30028, 83–91.

[23] Badur J., Kornet D., Sławiński D., Ziółkowski P.: *Analysis of unsteady flow forces acting on the thermowell in a steam turbine control stage*. J. Phys.: Conf. Ser. **760**(2016), 012001.

[24] Klimaszewski P., Zaniewski D., Witanowski Ł., Suchocki T., Klonowicz P., Lampart P.: *A case study of working fluid selection for a small-scale waste heat recovery ORC system*. Arch. Thermodyn. **40**(2019), 3, 159–180.

[25] Ziółkowski P., Badur J., Ziółkowski P.J.: *An energetic analysis of a gas turbine with regenerative heating using turbine extraction at intermediate pressure – Brayton cycle advanced according to Szewalski's idea*. Energy **185**(2019), 763–786.

[26] Głuch S., Piwowarski M.: *Enhanced master cycle – significant improvement of steam rankine cycle*. In: Proc. 25th Int. Conf. Engineering Mechanics 2019, Vol. 25 (I. Zolotarev, V. Radolf, Eds.), Svratk,13–16 May, 2019, 125–128.

[27] Kowalczyk T., Badur J., Ziółkowski P.: *Comparative study of a bottoming SRC and ORC for Joule–Brayton cycle cooling modular HTR exergy losses, fluid-flow machinery main dimensions, and partial loads*. Energy **206**(2020), 118072.

[28] Perycz S.: *Steam and Gas Turbines*. Wyd. Polit. Gdańskiej, Gdańsk 1988 (in Polish).

[29] https://www.ansys.com/products/fluids/ansys-cfx (accessed 15 Jan. 2021).

[30] Menter F.R., Kuntz M., Langtry R.: *Ten years of industrial experience with the SST turbulence model*. In: Proc. 4th Int. Symp.on Turbulence, Heat and Mass Transfer (K. Hajalič, Y. Nagano, M. Tummers, Eds.). Begell House, West Redding 2003, 625–632.

[31] Lemmon E. W., Huber M. L. & McLinden M.O.: *NIST Standard Reference Database 23*. In: Reference Fluid Thermodynamic and Transport Properties-REFPROP, Version 8.0, User's Guide, Standard Reference Data Series (NIST NSRDS), National Institute of Standards and Technology, Gaithersburg 2010.

[32] Wilcox D.C.: *Turbulence Modeling for CFD*. DCW Industries, La Canada 1998.

[33] Kornet S., Ziółkowski P., Jóźwik P., Ziółkowski P.J., Stajnke M., Badur J.: *Thermal-FSI modelling of flow and heat transfer in a heat exchanger based on minichannels*. J. Power Technol. **97**(2017), 5, 373–381.

[34] Badur J., Charun H.: *Selected problems of heat exchange modelling in pipe channels with ball turbulisers*. Arch. Thermodyn. **28**(2007), 3, 65–87.